Neurotransplantation of magnetically labeled oligodendrocyte progenitors: Magnetic resonance tracking of cell migration and myelination

J. W. M. Bulte[†‡], S.-C. Zhang[§], P. van Gelderen[¶], V. Herynek[‖], E. K. Jordan[†], I. D. Duncan[§**], and J. A. Frank[†**]

[†]Laboratory of Diagnostic Radiology Research Clinical Center, [¶]In Vivo NMR Center and [‖]Neuroimaging Branch, National Institute of Neurological Disorders and Stroke, National Institutes of Health, Bethesda, MD 20892; and [§]Department of Medical Sciences, School of Veterinary Medicine, University of Wisconsin, Madison, WI 53706

Edited by Solomon H. Snyder, Johns Hopkins University School of Medicine, Baltimore, MD, and approved November 5, 1999 (received for review August 20, 1999)

Demyelination is a common pathological finding in human neurological diseases and frequently persists as a result of failure of endogenous repair. Transplanted oligodendrocytes and their precursor cells can (re)myelinate axons, raising the possibility of therapeutic intervention. The migratory capacity of transplanted cells is of key importance in determining the extent of (re)myelination and can, at present, be evaluated only by using invasive and irreversible procedures. We have exploited the transferrin receptor as an efficient intracellular delivery device for magnetic nanoparticles, and transplanted tagged oligodendrocyte progenitor cells into the spinal cord of myelin-deficient rats. Cell migration could be easily detected by using three-dimensional magnetic resonance microscopy, with a close correlation between the areas of contrast enhancement and the achieved extent of myelination. The present results demonstrate that magnetic resonance tracking of transplanted oligodendrocyte progenitors is feasible; this technique has the potential to be easily extended to other neurotransplantation studies involving different precursor cell types.

Demyelination is an important pathological component of multiple sclerosis and other neurological disorders. Recent research has suggested that it is possible to promote (re)myelination in animal models of abnormal myelination or demyelination (1–3), either by endogenous oligodendrocytes or exogenous myelinating cells. The latter repair mechanism has received particular attention, because it has been shown that transplanted oligodendrocyte precursor cells can myelinate large areas in the central nervous system (4). A similar therapeutic approach in humans may be pursued and is supported by the safety and effectiveness of human neurotransplantation studies (5, 6). The clinical outcome of such studies will be directly determined by the extent of myelination, and thus by the immediate dispersion, migratory capacity, and long-term survival of grafted cells. A technique that could monitor the grafted cell migration continuously and noninvasively is crucial to guide further advances in neurotransplantation research. We hypothesized that tagging grafted cells with a magnetic label might allow magnetic resonance (MR) tracking of their migratory capacity, not unlike an earlier MR microscopy study that used labeled progeny cells to follow cell movements and lineages in the developing embryo (7). Magnetically labeled cells previously have received interest to study neural grafting procedures (8, 9) and cellular trafficking (10–13) by MR imaging.

Oligodendrocyte progenitors have a greater migratory and myelinating capacity than mature glial cells (14, 15). We therefore chose the rat oligodendrocyte progenitor cell line CG-4 (16, 17) as the graft, with the myelin-deficient (*md*) rat as a recipient, because the migration pattern of $LacZ^+$ CG-4 cells has been documented in detail with this model (18). The *md* rat carries an X-linked recessive mutation in the proteolipid protein gene and is characterized by an almost complete absence of myelin (19). We show here that, during their normal expansion in culture, CG-4 cells can be made highly magnetic by simple incubation of magnetic nanoparticles that are targeted to the transferrin receptor (Tfr). After neurotransplantation, these cells fully retained their migratory and myelinating capicity *in vivo*, could be easily detected by MR imaging, and allowed three-dimensional mapping of the achieved extent of myelination.

Materials and Methods

Preparation of Tfr-Targeted Magnetic Nanoparticles. Using the periodate-oxidation and borohydride reduction method, the alcohol groups of the dextran-coated MION-46-L were covalently linked to the terminal amine groups of OX-26. MION-46-L in 0.01 M citrate buffer, pH 8.4 first was oxidized at 4°C for 24 hr with 1 mg $NaIO_4$ per mg Fe. MION-46-L then was purified by using a Sephadex G-100 column, removing any unbound or released free dextran. OX-26 in 0.2 M sodium bicarbonate buffer, pH 6.5 was allowed to form Schiff's bases with MION-46L at 4°C for 16 h at a 1:1 protein/Fe weight ratio. The unstable Schiff's bases were reduced to secondary amide bonds by adding 1 mg of $NaCNBH_3$ per mg Fe and incubation at room temperature for 4 h, and the resulting MION-46L-OX-26 was purified over a Sephadex G-100 column.

Magnetic Labeling. CG-4 cells were cultured in the presence of 30% B104-conditioned medium as described (16). Cells were incubated with 2, 3, 6, 12, 25, or 50 μg Fe/ml MION-46L-OX-26 and 50 or 500 μg Fe/ml unconjugated MION-46L for 48 h. The cell density during incubation was approximately $2.5–3.0 \times 10^5$ per ml medium and per 15 cm^2 growth surface area (near confluent). Cells were trypsinized and washed three times for further analysis and transplantation. For Prussian blue staining, cytospins were fixed with 4% glutaraldehyde, washed, incubated for 30 min with 2% potassium ferrocyanide (Perls' reagent) in 6% HCl, washed, and counterstained with nuclear fast red. For immunoperoxidase staining, cytospins were fixed with acetone, washed, incubated with rabbit-anti-mouse Ig-horseradish peroxidase (Dako P260, 1:20 diluted, with addition of 3% normal rat serum) for 45 min at room temperature, washed, incubated with 0.2 mg/ml solubilized 3-amino-9-ethyl-carbazole in 0.05 M acetate buffer, pH 4.9 + 0.03% H_2O_2 for 10 min, washed, and counterstained with Mayer's haematoxylin. To determine the

This paper was submitted directly (Track II) to the PNAS office.

Abbreviations: *md*, myelin-deficient; MR, magnetic resonance; Tfr, transferrin receptor; TE, interecho time.

[‡]To whom reprint requests should be addressed at: Laboratory of Diagnostic Radiology Research, National Institutes of Health, Building 10, Room B1N256, 10 Center Drive, MSC 1074, Bethesda, MD 20892-1074. E-mail: jwmbulte@helix.nih.gov.

**I.D.D. and J.A.F. and their laboratories contributed equally to this work.

The publication costs of this article were defrayed in part by page charge payment. This article must therefore be hereby marked "*advertisement*" in accordance with 18 U.S.C. §1734 solely to indicate this fact.

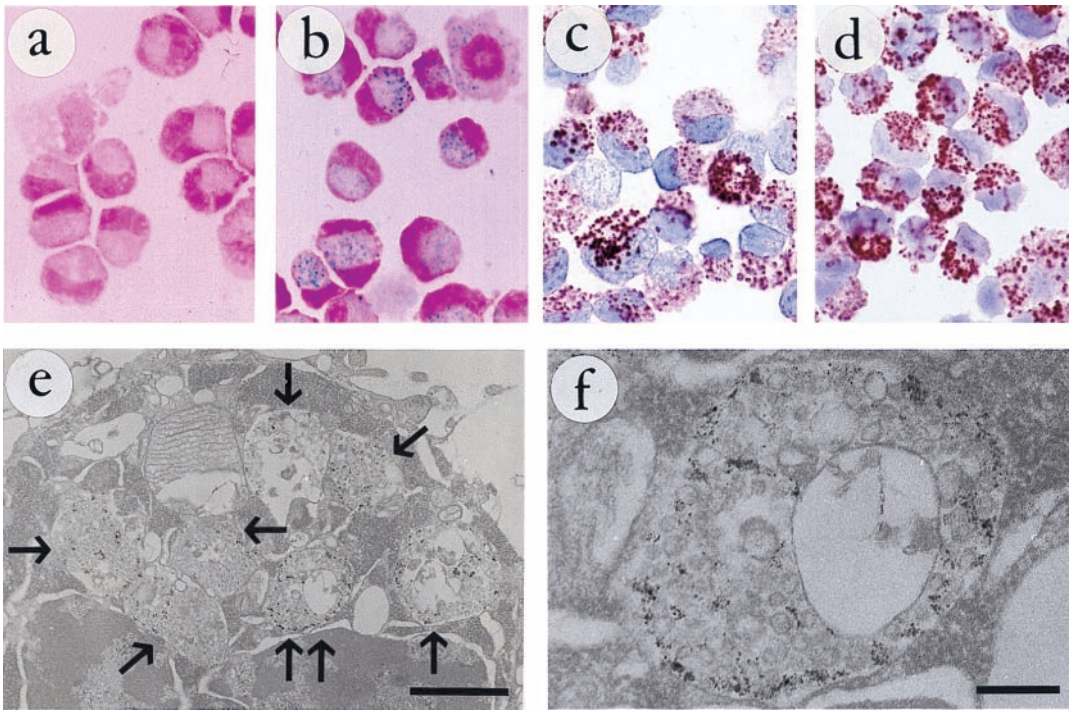

Fig. 1. (*a*) CG-4 cells labeled for 48 h with 0.5 mg Fe/ml unconjugated MION-46L. No particle uptake can be detected by using the Prussian blue stain for ferric iron. (*b–d*) CG-4 cells labeled for 48 h with 0.05 mg Fe/ml MION-46L-OX-26. (*b*) numerous iron-containing vesicles are visible. These vesicles also contain the covalently linked, endocytosed OX-26 mAb, as visualized in *c* by using immunoperoxidase staining. Under these conditions the total Tfr binding capacity for OX-26 appears nearly saturated, given the similar staining pattern in *d* by using additional OX-26 mAb added afterward. (e) Transmission electron microscopy of MION-46L-OX-26-tagged CG-4 cells reveals the presence of numerous vesicles (arrows), which measure approximately 0.6–1.0 μm in diameter, and which are filled with the electron-dense magnetic nanoparticles. One of the vesicles (double arrows) is shown at a higher magnification in *f* to demonstrate the association of particles with a (reversed) endocytosed membrane. All cells in *a–f* were trypsinized before staining. (Bars represent 1 μm in *e* and 200 nm in *f*.)

relative saturation of OX-26-(MION-46L) uptake, some cytospins were incubated afterward with 20 μg/ml OX-26 for 60 min at room temperature, washed, and further processed as described above. Tagged, washed, and 4% glutaraldehyde-fixed CG-4 cells also were embedded in 2% agar and stained with 0.1% osmium tetroxide for 30 min and with 0.5% uranyl acetate overnight. Ultrathin sections were further stained with lead citrate and examined with a JEOL 100CX transmission electron microscope operating at 60 kV.

Variable-Field Relaxometry. Tagged, washed CG-4 cells were counted by using a hemocytometer, and 1×10^7 cells were resuspended in 500 μl 4% (wt/wt) gelatin (Sigma G-2500, 300 Bloom) + 0.02% NaN_3. Using a custom-designed variable field relaxometer (Southwest Research Institute, San Antonio, TX), spanning a Larmor frequency range of 1 to 64 MHz (corresponding to a field strength of 0.025–1.5 Tesla), the T1 was measured by using a saturation recovery pulse sequence. T2 was measured by using a Carr-Purcell-Meiboom-Gill pulse sequence with 500 echoes and an interecho time of 2, 4, 6, and 10 msec.

Transplantation. This study was conducted in accordance with institutional guidelines for the use and care of laboratory animals. CG-4 cells were incubated with 12 μg Fe/ml MION-46L-OX-26 for 48 h, trypsinized, washed three times, and counted. Using a 30-μm diameter micropipette, approximately 5×10^4 cells in 1.0 μl medium were grafted into the T13/L1 region of the spinal cord of 7-day-old *md* rats ($n = 5$) and 1 normal littermate. The place of inoculation was marked with charcoal. Grafting experiments with unlabeled cells ($n = 5$) and magnetically labeled cells that were fixed with paraformaldeyde ($n = 2$) were included as controls.

MR Imaging and Histopathological Correlation. Rats were perfused with 4% paraformaldehyde, and spinal cords were dissected and further fixated for several days. Samples were placed in 5-mm NMR tubes filled with the perfluoroether Fomblin LC08 (Ausimont, Thorofare, NJ). Three-dimensional multigradient echo MR images were obtained at 52- or 78-μm isotropic resolution by using a 4.7 T Varian INOVA NMR spectrometer and a 6-mm diameter Bruker saddle coil. The scan parameters were: field of view, $20 \times 5 \times 5$ mm; matrix, $384 \times 96 \times 96$ or $256 \times 64 \times 64$; number of excitations, 100; repetition time 100 msec; interecho time (TE), 2.5 or 6 msec; *n* echoes, 6; flip angle, 30°. From the raw dataset, both amplitude images, quantitative R2* maps, and differential phase maps were created by using IDL processing software. After MR imaging, the (fixed) spinal cord specimens were cryoprotected and cut at 12-μm slice thickness. Sequential sections were stained for iron by using the Prussian blue reaction, for myelin by using antiproteolipid protein antibody, for astrocytes by using anti-glial fibrillary acidic protein antibody, and for microglia by using isolectin B4 as described (20, 21).

Results

Magnetic Labeling of Oligodendrocyte Progenitors. As magnetic label, MION-46L nanoparticles (22) were used throughout this study. MION-46L is a dextran-coated nanocolloid with a superparamagnetic maghemite- or magnetite-like inverse spinel core structure, measuring 4.6 ± 1.2 nm in diameter. The overall particle size is 8–20 nm. We attempted to tag the CG-4 oligodendrocyte progenitor cell line by using two different approaches. First, we tested simple incubation of MION-46L alone. Here, uptake may occur either by fluid-phase endocytosis of nonopsonized particles or by receptor-mediated endocytosis of particles opsonized with proteins present in the medium (23, 24).

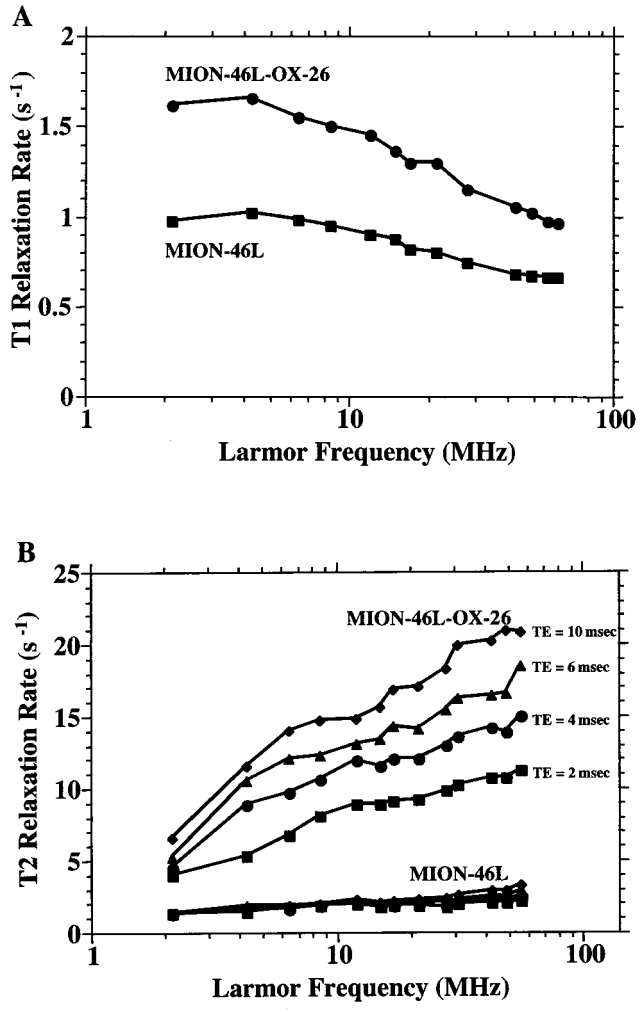

Fig. 2. 1/T1 (*A*) and 1/T2 (*B*) as function of Larmor frequency for MION-46L-labeled (0.5 mg Fe/ml) and MION-46L-OX-26-labeled (0.05 mg Fe/ml) cells. The dependence of 1/T2 on TE is indicative of (intra)cellular clustering of the magnetic nanoparticles.

The second approach involved specific targeting and endocytosis of particles by using the Tfr. Immunohistochemical staining of cultured CG-4 cells for Tfr expression showed an intense staining with the mAb OX-26 (25). This murine anti-rat Tfr mAb was produced after immunization with lectin-stimulated rat lymph node cells and is of the IgG2a isotype. OX-26 was covalently linked to MION-46L, and cultured CG-4 cells were incubated for 48 h with the Tfr-targeted (2–50 μg Fe/ml) as well as the unconjugated nanoparticles (50 and 500 μg Fe/ml), collected, washed, and further analyzed by (immuno)histochemical staining and transmission electron microscopy (TEM). No Prussian blue-positive product could be detected in cells incubated with MION-46L alone, even at a 10-fold higher concentration. In contrast, the OX-26-MION-46L-tagged cells demonstrated the presence of numerous intracellular vesicles that were filled with both magnetic nanoparticles and OX-26 mAb (Fig. 1 *a–d*). The similarity between the staining pattern for iron particles and the conjugated mAb suggests that, at 48 h after labeling, both components still remain intact and covalently linked. The TEM results were consistent with receptor-mediated endocytosis, with a reversal of the membrane upon endocytosis of the vesicle (Fig. 1 *e* and *f*). MION-46L-OX-26-tagged, washed CG-4 cells also were recultured for an additional 5 days. At this time point, cells were still dividing rapidly and retained many Prussian blue-positive vesicles. Because of the dilution effect of multiple cell divisions, the relative cellular number of these vesicles was reduced as compared with cells that were not recultured.

The Tfr-targeted uptake was further analyzed by using variable field T1-T2 relaxometry. Cells were homogeneously suspended in a tissue-mimicking gel at a fixed number of 2×10^7/ml. The mechanism by which magnetopharmaceuticals induce MR contrast is by increasing the longitudinal (T1) or transverse (T2) relaxation rate of protons; both can be directly measured. No significant increase of relaxation rates could be observed for unconjugated MION-46L-incubated cells. Over the entire frequency range, the OX-26-MION-46L-incubated cells showed a small, but significant, increase of 1/T1 (Fig. 2*A*) that was about double the values obtained for unconjugated MION-46L. The difference for the 1/T2 values of OX-26-MION-46L-incubated cells was much more pronounced, with an increase with frequency that was TE-dependent (Fig. 2*B*). There was a dose-dependent increase of the intensity of the Prussian blue-positive vesicles as well as the magnitude of the 1/T1 and 1/T2 relaxation rates. However, even at the lowest tested dose of 2 μg Fe/ml MION-46L-OX26, the CG-4 cells showed an abundance of iron- and OX-26-containing vesicles, with 1/T2 relaxation rates in the order of 10 s^{-1} (for TE = 6 msec) at 1.5 Tesla, compared with control values of about 1 s^{-1}. Trypan blue exclusion staining showed a similar viability for magnetically labeled and nonlabeled cells at all MION-46L-OX26 doses tested.

MR Tracking of Magnetically Labeled Cells. Magnetically labeled CG-4 cells were grafted into the spinal cord of neonatal *md* rats and normal littermates. Grafting experiments with unlabeled cells and cells that were labeled but subsequently fixed with paraformaldehyde were included as controls. At either 10 (n = 4) or 14 (n = 9) days after transplantation, the spinal cord was removed and further processed for three-dimensional high-resolution MR imaging. To obtain a completely dark background we embedded the specimens in a perfluoropolyether devoid of proton signals. This polymer was found to be inert, effectively sealing the specimens from dehydration, with no observed effects on tissue morphology. MR microscopy showed extensive migration (up to 8.4 mm) of grafted cells, particularly in the area of the dorsal column (Figs. 3*a* and 4*a*). The migration distance for the one normal littermate studied was 10.1 mm (not shown), suggesting that the presence of normal myelin and functional oligodendrocytes does not impede the migration of grafted CG-4 cells in the early developing central nervous system. In the unlabeled cell (control) graft MR images, no contrast could be observed except a fine hairline representing the 30-μm track of the micropipette, although a similar extensive myelination was present in the dorsal funiculus. The labeled dead cell control experiments showed contrast only at the injection site (Fig. 5); the area of contrast was less than 0.3 mm, and no spread could be observed. This finding implies that, even at 14 days postinjection, the iron particles remain localized and are not taken up and redistributed by other cells. Calculated differential MR phase maps proved that the contrast enhancement is caused by dephasing of proton spins in areas of different magnetic field gradients. These areas also correlated directly with calculated 1/T2* maps (both not shown).

The MR images were further correlated with histopathological staining for iron, myelin, astrocytes (glial fibrillary acidic protein, GFAP), and microglia. Both the Prussian blue and myelin staining matched closely the area of contrast enhancement seen on the MR images (Figs. 3 *b* and *c* and 4 *b* and *c*). Because the Prussian blue reaction did not overlap with GFAP and isolectin B4 staining (not shown), the MION-46L had not been redistributed into astrocytes or microglia cells. The mor-

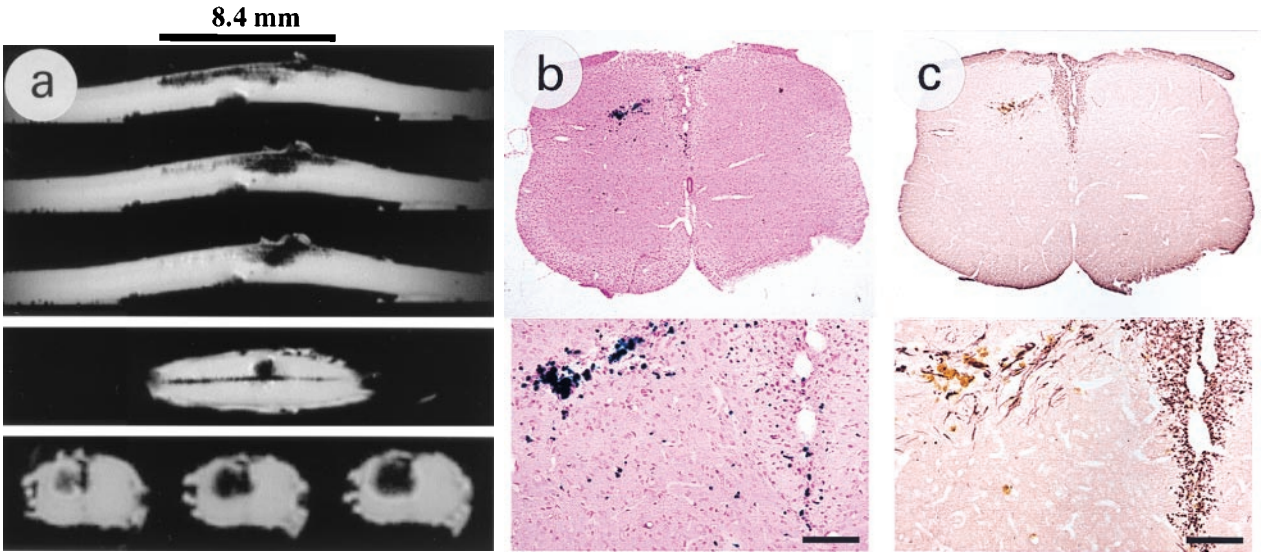

Fig. 3. *Md* rat 10 days after transplantation of magnetically labeled CG-4 cells. (*a*) Shown are the three MRI planes of view for TE = 6 msec at 78 μm isotropic resolution. In the sagittal plane (top images, consecutive slices), cellular migration can be appreciated over a distance of 8.4 mm. The contrast in the transverse images (enlarged in bottom row, shown is each third interleaved slice) corresponds to the area of Prussian blue staining (*b Upper*) and antiproteolipid protein immunolabeling (*c Upper*) and shows a blooming effect caused by an extended-range susceptibility effect of the magnetic particles. (*b* and *c Lower*) Cell migration from the injection site toward the dorsal column, where the majority of the newly formed myelin was found. Note the differential orientation of the individual myelin fibers, which is along the direction of CG-4 cell migration. (Bars represent 100 μm in *b* and *c Lower*.)

phology of iron-containing cells resembled that of oligodendrocytes, with a small cell body and multiple processes (Fig. 4*d*).

Discussion

Our study introduces MR tracking as a technique to monitor, noninvasively and in three dimensions, the migratory capacity of magnetically labeled cells after transplantation. As magnetic label we used superparamagnetic iron oxides, which are, on a millimolar metal basis, the most MR-sensitive labels currently available (26, 27). These particles possess a large ferrimagnetic moment that, because of the small crystal size, is free to align with an applied magnetic field (i.e., there is no hysteresis), hence the term superparamagnetic. The aligned magnetization then creates microscopic field gradients that dephase nearby protons and enhance the T2 NMR relaxation rate, over and beyond the usual dipole-dipole relaxation mechanism that affects both T1

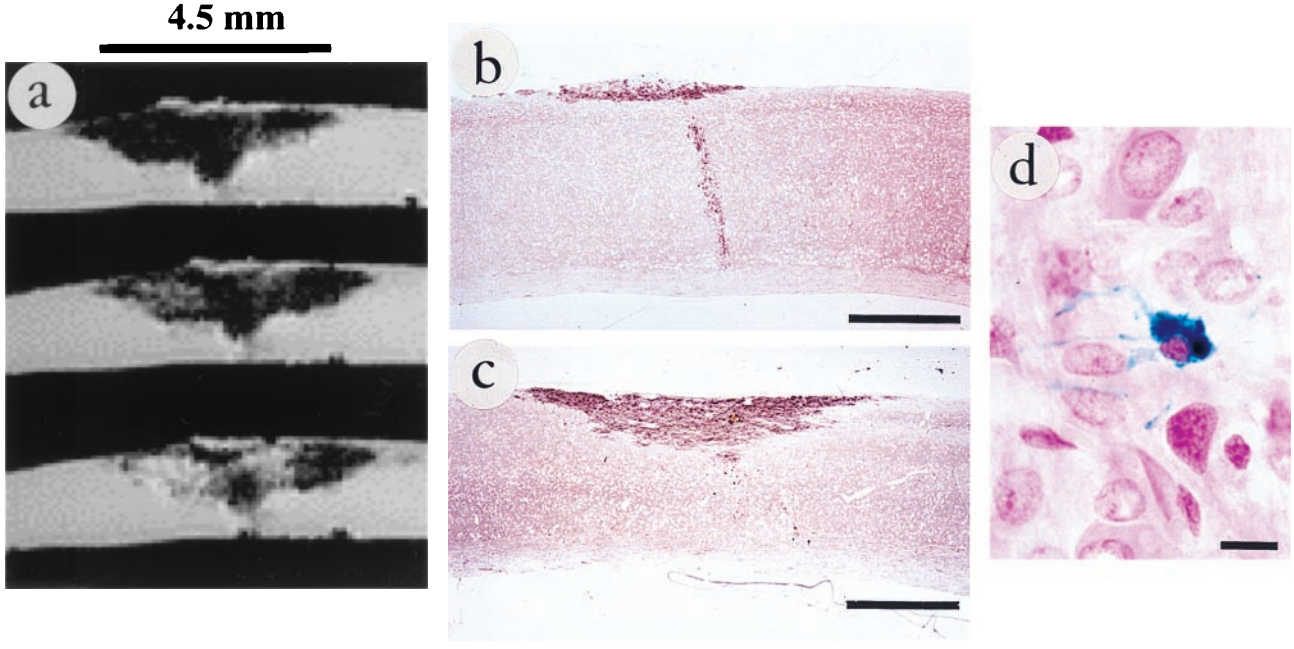

Fig. 4. *Md* rat 14 days after transplantation. Shown is the sagittal MRI plane for TE = 6 msec (*a*, consecutives slices) at 78-μm isotropic resolution, with cellular migration over a distance of 4.5 mm. The antiproteolipid protein immunolabeling (*b* and *c*) show that the observed MRI contrast corresponds closely to the myelination. In *b*, note the injection track with cell migration toward the dorsal column (the spherical appearance of the injection track in the MR images is the result of its direction relative to the orientation of the external magnetic field gradient). Prussian blue-positive cells (*d*) in the area of new myelination resembled the cellular morphology of oligodendrocytes. (Bars represent 1 mm in *b* and *c* and 10 μm in *d*.)

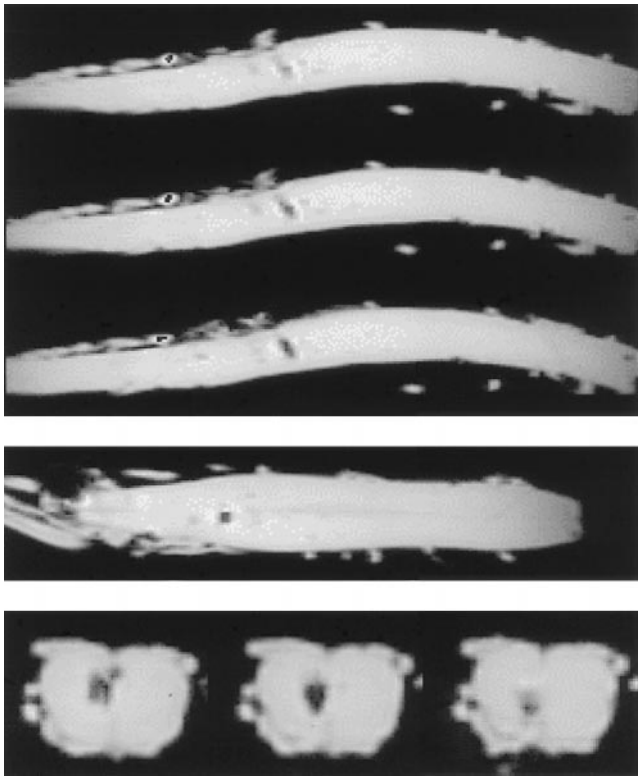

Fig. 5. *Md* rat 14 days after transplantation of magnetically labeled and paraformaldehyde-fixed (dead) CG-4 cells. Shown are the three MRI planes of view for TE = 6 msec, with consecutive slices for the sagittal plane (top images) and interleaved slices for the transverse plane (bottom row, enlarged). In this control experiment, contrast is visible at the injection site only; no cellular migration can be observed. Magnifications: ×4, *Top* and *Middle*.

and T2 relaxation times. We decided to use MION-46L as our (superpara)magnetic label of choice because of (*i*) its biocompatibility, monocrystallinity, and small size, (*ii*) its well-understood magnetic properties and effect on NMR relaxation (28, 29), and (*iii*) its proven ability to form covalent bonds with mAbs (30, 31). We exploited the Tfr to shuttle MION-46L nanoparticles into cultured CG-4 cells. These cells appeared to express high Tfr numbers, in agreement with an earlier study of immature oligodendrocytes (32). The Tfr has the ability of being recycled (back to the cell membrane) within minutes after endocytosis, allowing multiple delivery of (magneto)pharmaceuticals through use of a single receptor. Using transferrin-conjugated drugs, the Tfr therefore has been used extensively as a cellular drug delivery system (33). Alternatively, anti-Tfr mAbs mimicking the binding of transferrin could be used, and we decided to pursue the latter approach, although it is not clear whether anti-Tfr mAbs dissociate within the cell and recycle at the same rate as transferrin(-conjugated ligands). OX-26 is an internalizing mAb that binds noncompetitively with transferrin and previously has been shown to be very effective in shuttling OX-26-conjugated drugs into cells across an intact blood–brain barrier (34–37). Indeed, the use of OX-26-conjugated magnetic nanoparticles allowed the preparation of cells that were magnetically very highly loaded, yet they fully retained their migratory and myelinating capacity *in vivo*, and as such did not behave differently from unlabeled cells. A high magnetic loading factor is absolutely necessary to induce changes in MRI signal; the overall sensitivity of MR imaging for molecular or cellular tracers is low and about 3 orders of magnitude lower than other conventional nuclear imaging techniques, e.g., positron-emission tomography, single photon-emission computed tomography, or γ-camera imaging. For the magnetically labeled cells, we observed a TE dependence and enhancement of proton spin dephasing. Because of their nanometer size, this effect normally is not seen in simple MION-46L solutions. The TE dependence is indicative of (intra)cellular clustering; in this micrometer size regime, either the endocytosed vesicles or the cells themselves act as one larger particle that causes additional macroscopic field gradients for the diffusing water protons. The 1/T2:1/T1 ratio of about 10 at 1.5 Tesla is therefore several-fold larger than the value seen for noncell bound MION-46L in solution (28). These additional field gradients increase the sensitivity of gradient echo MR imaging for magnetic tracers. In fact, it sometimes can be so sensitive that water protons at distant sites are affected, leading to a "blooming effect" and can be appreciated to have occurred for the injection site for the transverse images in Fig. 3*a*. Another factor that may potentially affect the (late-term) sensitivity of MR detection is the proliferation rate of the magnetically tagged cells, with the internalized label presumably being divided into progeny cells, effectively diluting out the magnetic tag. Oligodendrocyte progenitor cells, however, stop dividing and go in a resting state once they myelinate.

We observed an excellent agreement between the areas of MR contrast enhancement and histopathological stainings for iron and newly formed myelin. The transplanted CG-4 cells appeared to have migrated almost exclusively within the dorsal column. This finding is in agreement with an earlier report (18) that used the same cell line and transplantation model and in which a migration distance of up to 7 mm was observed at 2 weeks after transplantation. Our MR tracking data of 4.5- to 8.4-mm migration are consistent with those results. Our approach thus may be applied to accurately determine the achieved extent of (re)myelination and to investigate, on a continuous, noninvasive basis, the various factors that may either promote or inhibit a widespread global myelination (38).

This work also may have important implications for future studies involving transplantation of other glial cells, oligodendrocytes, neurons, and, in particular, neural stem cells (38–42). Further progress in this field has been hampered by a lack of suitable methods for studying the *in vivo* efficiency and migration of grafted cells. Because the Tfr is a ubiquitous receptor present on many neural cells in high numbers, the Tfr-targeted magnetic labeling presented here may be easily extended to other neurotransplantation studies. We believe that MR tracking of grafted cells may become a powerful tool for understanding the molecular mechanisms that are ultimately responsible for a successful migration and expansion of neurotransplanted cells *in vivo*.

We are grateful to Drs. W. Jefferies and A. Like and the Medical Research Council Cellular Immunity Unit, University of Oxford, for providing the OX-26 hybridoma, Dr. R. Weissleder for preparing the MION-46L, and Drs. L. D. Hudson and H. F. McFarland for critically reviewing the manuscript. We also thank B. Ge, J. Henderson, C. Janssen, and A. Olson for their invaluable help and assistance with this study. This work is partially supported by the National Institutes of Health Intramural Research Program and grants from the National Institutes of Health (NS 33710), the Myelin Project, and the Oscar Rennebohm Foundation.

1. Blakemore, W. F., Franklin, R. J. M. & Noble, M. (1996) in *Glial Cell Development: Basic Principles and Clinical Relevance*, eds. Jessen, K. R. & Richardson, W. D. (BIOS Scientific, Oxford), pp. 209–220.
2. Miller, D. J., Asakura, K. & Rodriguez, M. (1996) *Brain Pathol.* **6,** 331–344.
3. Duncan, I. D., Grever, W. E. & Zhang, S.-C. (1997) *Mol. Med. Today* **3,** 554–561.
4. Duncan, I. D. & Milward, E. A. (1995) *Brain Pathol.* **5,** 301–310.
5. Lindvall, O., Brundin, P., Widner, H., Rehncrona, S., Gustavii, B., Frackowiak, R., Leenders, K. L., Sawle, G., Rothwell, J. C., Marsden, C. D., *et al.* (1990) *Science* **247,** 574–577.
6. Kordower, J. H., Freeman, T. B., Snow, B. J., Vingerhoets, F. J. G., Mutson,

E. J., Sanberg, P. R., Hauser, R. A., Smith, D. A., Nauert, G. M., Perl, D. P., *et al*. (1995) *N. Engl. J. Med.* **332,** 1118–1124.
7. Jacobs, R. E. & Fraser, S. E. (1994) *Science* **263,** 681–684.
8. Norman, A. B., Thomas, S. R., Pratt, R. G., Lu, S. Y. & Norgren, R. B. (1992) *Brain Res.* **594,** 279–283.
9. Hawrylak, N., Ghosh, P., Broadus, J., Schlueter, C., Greenough, W. T. & Lauterbur, P. C. (1993) *Exp. Neurol.* **121,** 181–192.
10. Bulte, J. W. M., Ma, L. D., Magin, R. L., Kamman, R. L., Hulstaert, C. E., Go, K. G., The, T. H. & de Leij, L. (1993) *Magn. Reson. Med.* **29,** 32–37.
11. Yeh, T.-C., Zhang, W., Ildstad, S. T. & Ho, C. (1995) *Magn. Reson. Med.* **33,** 200–208.
12. Bulte, J. W. M., Laughlin, P. G., Jordan, E. K., Tran, V. A., Vymazal, J. & Frank, J. A. (1996) *Acad. Radiol.* **3,** S301–S303.
13. Schoepf, U., Marecos, E. M., Melder, R. J., Jain, R. K. & Weissleder, R. (1998) *BioTechniques* **24,** 642–651.
14. Warrington, A. E., Barbarese, E. & Pfeiffer, S. E. (1993) *J. Neurosci. Res.* **34,** 1–13.
15. Archer, D. R., Cuddon, P. A., Lipsitz, D. & Duncan, I. D. (1997) *Nat. Med.* **3,** 54–59.
16. Louis, J. C., Magal, E., Muir, D., Manthorpe, M. & Varon, S. (1992) *J. Neurosci. Res.* **31,** 193–204.
17. Louis, J. C., Magal, E., Takayama, S. & Varon, S. (1993) *Science* **259,** 689–692.
18. Tontsch, U., Archer, D. R., Dubois-Dalcq, M. & Duncan, I. D. (1994) *Proc. Natl. Acad. Sci. USA* **91,** 11616–11620.
19. Dentinger, M. P., Barron, K. D. & Csiza, C. K. (1982) *J. Neurocytol.* **11,** 671–679.
20. Zhang, S.-C., Lundberg, C., Lipsitz, D., O'Connor, L. T. & Duncan, I. D. (1998) *J. Neurocytol.* **27,** 475–489.
21. Zhang, S.-C., Ge, B. & Duncan, I. D. (1999) *Proc. Natl. Acad. Sci. USA* **96,** 4089–4094.
22. Shen, T., Weissleder, R., Papisov, M., Bogdanov, A., Jr., & Brady, T. J. (1993) *Magn. Reson. Med.* **29,** 599–604.
23. Weissleder, R., Cheng, H.-C., Bogdanova, A. & Bogdanov, A., Jr. (1997) *J. Magn. Reson. Imaging* **7,** 258–263.
24. Moore, A., Weissleder, R. & Bogdanov, A., Jr. (1997) *J. Magn. Reson. Imaging* **7,** 1140–1145.
25. Jefferies, W. A., Brandon, M. R., Hunt, S. V., Williams, A. F., Gatter, K. C. & Mason, D. Y. (1984) *Nature (London)* **312,** 162–163.
26. Weissleder, R., Bogdanov, A., Neuwelt, E. A. & Papisov, M. (1995) *Adv. Drug Del. Rev.* **16,** 321–334.
27. Bulte, J. W. M. & Brooks, R. A. (1997) in *Scientific and Clinical Applications of Magnetic Carriers*, eds. Häfeli, U., Schütt, W., Teller, J. & Zborowski, M. (Plenum, New York), pp. 527–543.
28. Bulte, J. W. M., Brooks, R. A., Moskowitz, B. M., Bryant, L. H., Jr. & Frank, J. A. (1999) *Magn. Reson. Med.* **42,** 379–384.
29. Roch, A., Muller, R. N. & Gillis, P. (1999) *J. Chem. Phys.* **110,** 5403–5411.
30. Weissleder, R., Lee, A. S., Khaw, B. A., Shen, T. & Brady, T. J. (1992) *Radiology* **182,** 381–385.
31. Remsen, L. G., McCormick, C. I., Roman Goldstein, S., Nilaver, G., Weissleder, R., Bogdanov, A., Hellstrom, K. E., Hellstrom, I., Kroll, R. A. & Neuwelt, E. A. (1996) *Am. J. Neuroradiol.* **17,** 411–418.
32. Lin, H. H. & Connor, J. R. (1989) *Dev. Brain Res.* **49,** 281–293.
33. Wagner, E., Curiel, D. & Cotton, M. (1994) *Adv. Drug Del. Rev.* **14,** 113–135.
34. Friden, P. M., Walus, L. R., Musso, G. F., Taylor, M. A., Malfroy, B. & Starzyk, R. M. (1991) *Proc. Natl. Acad. Sci USA* **88,** 4771–4775.
35. Friden, P. M., Walus, L. R., Watson, P., Doctrow, S. R., Kozarich, J. W., Backman, C., Bergman, H., Hoffer, B., Bloom, F. & Granholm, A. C. (1993) *Science* **259,** 373–377.
36. Huwyler, J., Wu, D. & Pardridge, W. M. (1996) *Proc. Natl. Acad. Sci. USA* **93,** 14164–14169.
37. Pardridge, W. M. (1999) *Adv. Drug Del. Rev.* **36,** 299–321.
38. Yandava, B. D., Billinghurst, L. L. & Snyder, E. Y. (1999) *Proc. Natl. Acad. Sci. USA* **96,** 7029–7034.
39. McKay, R. (1997) *Science* **276,** 66–71.
40. Brüstle, O., Choudhary, K., Karram, K., Huttner, A., Murray, K., Dubois-Dalcq, M. & McKay, R. D. G. (1998) *Nat. Biotechnol.* **16,** 1040–1044.
41. Eriksson, P. S., Perfilieva, E., Bjork-Eriksson, T., Alborn, A. M., Nordborg, C., Peterson, D. A. & Gage, F. H. (1998) *Nat. Med.* **4,** 1313–1317.
42. Brüstle, O., Jones, K. N., Learish, R. D., Karram, K., Choudhary, K., Wiestler, O. D., Duncan, I. D. & McKay, R. D. G. (1999) *Science* **285,** 754–756.